



# 1 **Bedload transport measurements with Swiss impact plate geophones** 2 **in two Austrian mountain streams (Fischbach and Ruetz): system** 3 **calibration, grain size estimation, and environmental signal pick-up**

4 Dieter Rickenmann<sup>1</sup>, Bruno Fritschi<sup>1</sup>

5 <sup>1</sup>Swiss Federal Research Institute WSL, Birmensdorf, 8903, Switzerland

6 *Correspondence to:* Dieter Rickenmann (dieter.rickenmann@wsl.ch)

## 7 **Abstract.**

8 The Swiss plate geophone system is a bedload surrogate measuring technique that has been installed in more than 20  
9 streams, primarily in the European Alps. Here we report about calibration measurements performed in two mountain streams  
10 in Austria. The Fischbach and Ruetz gravel–bed streams are characterized by important runoff and bedload transport during  
11 the snowmelt season. A total of 31 (Fischbach) and 21 (Ruetz) direct bedload samples were obtained during a six year  
12 period. Using the number of geophone impulses and total transported bedload mass for each measurement to derive a  
13 calibration function, results in a strong linear relation for the Fischbach, whereas there is only a poor linear calibration  
14 relation for the Ruetz measurements. Instead, using geophone impulse rates and bedload transport rates indicates that two  
15 power law relations best represent the Fischbach data, depending on transport intensity; for lower transport intensities, the  
16 same power law relation is also in reasonable agreement with the Ruetz data. These results are compared with data and  
17 findings from other field sites and flume studies. We further show that the observed coarsening of the grain size distribution  
18 with increasing bedload flux can be qualitatively reproduced from the geophone signal, when using the impulse counts along  
19 with amplitude information. Finally, we discuss implausible geophone impulse counts that were recorded during periods  
20 with smaller discharges without any bedload transport, and that are likely caused by vehicle movement very near to the  
21 measuring sites.

## 22 **1 Introduction**

23 In the past decade or so, an increasing number of studies were undertaken on bedload surrogate acoustic measuring  
24 techniques which were tested both in flume experiments and in field settings. A review of such indirect bedload transport  
25 measuring techniques was recently published by Rickenmann (2017a, 2017b). Examples of measuring systems include the  
26 Japanese pipe microphone (Mizuyama et al., 2010a, 2010b; Uchida et al. 2013; Goto et al. 2014), the Swiss plate geophone  
27 (Rickenmann and Fritschi, 2010, Rickenmann et al. 2012, 2014), other impact plate systems (Krein et al., 2008, 2016; Møen  
28 et al. 2010; Reid et al. 2007; Beylich and Laute 2014; Taskiris et al. 2014), and hydrophones, i.e. underwater microphones  
29 (Barton et al. 2010; Camenen et al. 2012; Rigby et al. 2015). It is well known that bedload transport rates often show very



30 large variability for given flow conditions (Gomez, 1991; Leopold and Emmett, 1997; Ryan and Dixon, 2008; Recking,  
31 2010), and that prediction of (mean) bedload transport rates is still very challenging, particularly for steep and coarse-  
32 bedded streams (Bathurst et al., 1987; Nitsche et al., 2011; Schneider et al. 2015, 2016). For such conditions, direct bedload  
33 transport measurements are typically difficult to obtain, or may be impossible to make during high flow conditions (Gray et  
34 al., 2010). In contrast, indirect bedload transport measuring methods have the advantage of providing continuous monitoring  
35 data both in time and over a cross-sections, even during difficult flow conditions, and are therefore expected to increase our  
36 understanding of bedload transport.

37 A fair number of these measuring techniques have been successfully calibrated for total bedload flux, which generally  
38 requires contemporaneous direct bedload transport measurements in the field (Thorne, 1985, 1986; Voulgaris et al., 1995;  
39 Rickenmann and McArdell, 2007, 2008; Mizuyama et al. 2010b; Rickenmann et al. 2014; Mao et al., 2016; Habersack et al.  
40 2016; Kreisler et al. 2016). Essentially, linear or power law relations were established between a simple metric  
41 characterizing the acoustic signal and bedload mass. In some studies further calibration relations were established to identify  
42 particle size, either based on signal amplitude (Mao et al., 2016; Wyss et al., 2016a) and/or on characteristic frequency of  
43 that part of the signal which is associated with a single impact of a particle (e.g. for impact plate systems; Wyss et al., 2016b)  
44 or by determining a characteristic frequency for an entire grain size mixture (for the hydrophone system; Barrière et al.,  
45 2015a). A few of the acoustic measuring techniques were used to determine bedload transport by grain size classes (Mao et  
46 al., 2016; Wyss et al., 2016a). Finally, some studies examined to what extent findings from flume experiments can be  
47 quantitatively transferred and applied to field sites for which independent, direct calibration measurements exist (Mao et al.,  
48 2016; Wyss et al., 2016b, 2016c).

49 In this study we report on calibration measurements of the Swiss plate geophone (SPG) system in two mountain streams  
50 in Austria. The Fischbach and Ruetz gravel-bed streams are characterized by important runoff and bedload transport during  
51 the snowmelt season. During a six year period, 31 (Fischbach) and 21 (Ruetz) direct bedload samples were obtained in the  
52 two streams, respectively. The objectives of this paper are: (i) to present and discuss different ways of analysing the  
53 geophone calibration measurements, also in comparison with data and findings from other field sites and flume studies; (ii)  
54 to show that the observed coarsening of the grain size distribution with increasing bedload flux can be qualitatively  
55 reproduced from the geophone signal; and (iii) to discuss implausible geophone impulse counts that were recorded during  
56 periods with small discharge and without any bedload transport, and that are probably associated with close-by vehicle  
57 movement.

## 58 **2 Field sites and calibration measurements**

### 59 **2.1 Overview of field sites and geophone measurements**

60 The first indirect bedload transport measurements using impact plates were made in the Erlenbach from 1986 to 1999 using a  
61 piezoelectric crystal as sensor, with the aim of continuously monitoring the intensity of bedload transport and its relation to



62 stream discharge (Bänziger and Burch, 1990; Rickenmann, 1994, 1997; Hegg et al., 2006; Rickenmann and McArde-  
63 2007). A geophone sensor was used at the Erlenbach and at all other field sites that were set up in the year 2000 and later  
64 (Rickenmann and Fritschi, 2010). In the meantime, the SPG system has been installed in more than 20 streams primarily in  
65 Central Europe (Rickenmann, 2017b). An array of steel plates is typically installed flush with the surface of a sill or check  
66 dam, a location where there is only a small chance for (substantial) deposition of bedload grains during transport conditions.

67 The Fischbach and Ruetz field sites were installed by the Tyrolean Hydropower Company (TIWAG). They are located in  
68 partly glaciated catchments in the Tyrolean Alps (Fig. 1), at elevations of 1544 m a.s.l. (Fischbach) and 1688 m a.s.l.  
69 (Ruetz). Thus, the streams have a nival runoff regime, with typical daily discharge variations and regular bedload transport  
70 during snow and glacier melt in spring and summer. At both field sites, water discharge and bedload transport have been  
71 monitored since 2008. The stream cross-section is essentially trapezoidal at both measuring sites, with the banks protected  
72 by riprap and inclined at 45° (Fig. 2, 3). The geophone sensors are fixed in a cylindrical aluminium case and are mounted on  
73 the underside and in the middle of stainless steel plates, which are screwed into supporting steel constructions (UPN profiles)  
74 and are acoustically isolated by elastomer elements. The steel plates are 0.360 m long, 0.496 m wide, and 0.015 m thick. The  
75 entire steel construction is 8.2 m long (transvers to the flow direction) and embedded into a concrete sill, founded two meters  
76 into the river bed. The entire concrete structure is 8.7 m wide, and it is laterally inclined at 5% to the river left side (Fig. 3),  
77 which improves the discharge measurements at low flows. The sill is protected with riprap on the up- and downstream side.  
78 Starting with the first steel plate located 0.35 m from the right bank, every second steel plate is equipped with a geophone  
79 sensor, so that there are a total of eight sensors at each site.

80 At both sites, the concrete sill is located 4 m downstream of the cross-section where flow stage is measured on the left  
81 side of the stream, and where flow velocity measurements are made by TIWAG to establish a flow rating curve. At the  
82 Fischbach, a bridge crosses the stream some 13 m upstream of the concrete sill, and provides vehicle access to the measuring  
83 hut on the left side on a small forest road with very infrequent traffic. Along the right side of the stream a local paved road  
84 passes nearby, situated only in 5 m horizontal and about 4.5 m vertical distance above the concrete sill with the geophone  
85 plates (Fig. 3). Uphill the road leads to the village of Gries with about 200 inhabitants. This is the only village to be accessed  
86 upstream of the measuring site. In winter it serves as a relatively small ski resort. At the Ruetz, a bridge crosses the stream  
87 some 15 m upstream of the concrete sill, and provides vehicle access to a large parking lot, paved with gravel, on both sides  
88 of the stream. The measuring site is located at Mutterbergalm in the Stubai valley. From there a cable car provides access to  
89 a large skiing area (winter) and to a hiking area (summer) in the mountains. The public road ends at Mutterbergalm. The  
90 parking lot is situated in a similar minimal distance to the measuring cross section as at the Fischbach, i.e. with about 5 m  
91 horizontal and 4.5 m to 5 m vertical distance above the concrete sill. This information is important for the analysis and  
92 interpretation of the pick-up of geophone signal by environmental sources other than bedload transport.



## 93 2.2 Direct bedload measurements for system calibration

94 At each of the two sites, a streamlined metal pillar was installed 0.5 m downstream of the plate with the geophone sensor no.  
95 5 to facilitate the calibration measurements. The metal pillar has a height of 2.5 m and a maximum width of 0.25 m and  
96 ensures that a pressure–difference type metal basket sampler fits snugly onto the bed and can be held in place during the  
97 bedload sampling operation (Fig. 2b). The aperture of the basket is 50 cm by 50 cm, the same width as the sensor plate. The  
98 basket has a notch (cut–out) at a downstream distance of 0.45 m from the aperture (Fig. S1, Supporting information). The  
99 notch is somewhat larger than the cross–section of the metal pillar, and the inside of the notch is equipped with rollers. This  
100 system allows an exact positioning of the basket during geophone calibration measurements. The maximum width of the  
101 basket is 0.90 m and the total length is 2.10 m. During operation the upper surface of the sampler is horizontal while the  
102 lower surface is declined at 15% in the downstream direction, in line with the artificial bed in the vicinity of the metal pillar.  
103 Over the 0.80 m tail–end of the sampler, the top and sidewall surfaces of the basket are made of 10 mm metal wire mesh.  
104 The total volume of the basket is about 0.91 m<sup>3</sup>.

105 The calibration measurements used here were obtained by TIWAG in both streams during the summer months of 2008 –  
106 2013 using the basket bedload sampler. A total of 31 measurements from the Fischbach and 21 measurements from the  
107 Ruetz were used in this analysis (Table 1). The maximum sample mass caught in the sampler was 518 kg (including particles  
108 finer than 10 mm) in the Fischbach; assuming a bulk density of 1600 kg m<sup>-3</sup>, the bedload volume of this sample was about  
109 0.32 m<sup>3</sup> or about a third of the total sampler volume. Four calibration measurements from the Fischbach could not be used  
110 due to overfilling of the sampler. The grain size distribution of the samples was determined by sieve analysis by a TIWAG–  
111 owned engineering consultant. A line–by–number analysis was performed in both streams in October 2012 to estimate the  
112 grain size distribution of the bed surface upstream of the geophone sites.

## 113 2.3 Signal pre–processing, recorded geophone values, and amplitude histogram analysis

114 The bedload impact shocks on the steel plate are transmitted to the geophone sensor and, thereby, an electrical potential is  
115 produced. The standard geophone sensor uses a magnet in a coil as an inductive element. The magnet picks up the vibrations  
116 of the steel plate and induces a current in the coil which is proportional to the velocity of the magnet. Whenever the voltage  
117 exceeds a preselected threshold amplitude value,  $A_{\min}$ , the shock is recorded as an impulse. Contrary to all the other sites  
118 equipped with an SPG system, the threshold amplitude value  $A_{\min}$  used to determine *IMP* values was set at 0.07 V at the  
119 Fischbach and Ruetz (Tables 2, 3). The reason is that the first regular geophone recordings in the Fischbach had shown  
120 maximum amplitudes in excess of 10 V, the upper limit of the recording system. To increase the resolution of large  
121 amplitudes, the raw signal was dampened by about 30%. To compensate for lower signal strength in relation to the impulse  
122 counts, the threshold amplitude value  $A_{\min}$  was also reduced by 30% when compared with a typical value of 0.1 V used at  
123 other sites.



124 At most of the field sites with SPG measurements, several signal summary values were routinely stored in the past. The  
125 most often used summary value for calibration purposes are the summed impulse counts *IMP*. These values were found to  
126 correlate reasonably well with bedload mass or volume transported (Rickenmann and McArdeU, 2007, 2008; Rickenmann et  
127 al., 2012, 2014). Another useful summary value is maximum amplitude *MaxA* that may be determined for different recording  
128 intervals. During calibration measurements, all summary values were typically stored in 1 second intervals. During normal  
129 flow monitoring, the recording interval for the summary values at the Fischbach and Ruetz was 15 minutes. (At other SPG  
130 measurement sites operated by WSL this recording interval is typically 1 minute).

131 Using the so-called amplitude histograms (AH), Wyss et al. (2016, 2014) demonstrated for the SPG measurements at the  
132 Erlenbach (Swiss Prealps) that absolute bedload masses for each grain size class could be successfully calculated for both the  
133 calibration and validation data obtained with the moving basket samplers. The continuous recording of AH data was also  
134 implemented at the Fischbach and Ruetz measuring sites, with a recording interval of 1 minute. At these sites, impulses were  
135 determined separately for 17 amplitude classes as listed in Table 2. For the analysis in this study, for each amplitude  
136 threshold value  $A_{th}$  (upper class boundary value) a corresponding particle size  $D$  was estimated according to an empirical  
137 relation given in Wyss et al. (2016c, Eq. 11) and reported in Appendix A as Eq. (A1).

### 138 3. Results

#### 139 3.1 Calibration relations for bedload mass and bedload flux using impulse counts

140 The following calibration relations and calibration coefficients were determined using the transported bedload mass  $M$ , for  
141 particles with  $D$  larger than 10 mm, the impulses *IMP* summed over the sampling period of duration  $T_s$ :

$$142 \quad M = k_{lin} IMP \quad (1)$$

$$143 \quad M = k_{pow} IMP^e \quad (2)$$

$$144 \quad k_{tot} = \Sigma M / \Sigma IMP \quad (3)$$

145 where the units are in [kg] for  $M$  and for the coefficients ( $k_{lin}$ ,  $k_{pow}$ ,  $k_{tot}$ ), and the  $\Sigma$  sign implies a summation over all the  
146 calibration measurements per site. Equations (1) and (2) were obtained from a linear regression (using log values in case of  
147 Eq. 2), while Eq. (3) represents a mean, linear calibration coefficient based on the total mass and the total number of  
148 impulses for all calibration measurements taken together. The resulting coefficients ( $k_{lin}$ ,  $k_{pow}$ ,  $k_{tot}$ ), exponents ( $e$ ) and  
149 statistical properties of the calibration relations are reported in Table 3. The squared correlation coefficient  $r^2$  was  
150 determined between the measured masses  $M$  and the estimated masses  $M_{reg}$  (using eq. 1, 2, or  $k_{tot}$  in eq. 2). The relative  
151 standard deviation  $s_{e,r}$  is determined for the ratios ( $M_{reg}/M$ ), using the regression relation to determine  $M_{reg}$  from the recorded  
152 impulses *IMP*.



153 For the Fischbach, the calibration relations in the form of Eqs. (1) and (2) show a rather high correlation coefficient (Fig.  
 154 4, Table 3), which is also characteristic for similar calibration relations determined for the Erlenbach (Rickenmann et al.,  
 155 2012, 2014). For the Ruetz, the calibration relations in the form of Eqs. (1) and (2) are less well defined (Fig. 5, Table 3).  
 156 Due to the inclusion of four additional calibration measurements obtained in 2012 and 2013, the correlation coefficient for  
 157 the Ruetz is lower than in an earlier analysis that used only 17 measurements from the period 2008 to 2011 (Rickenmann et  
 158 al., 2014). This level of correlation is similar to calibration measurements obtained for the Navisence stream in Switzerland  
 159 (Wyss et al., 2016c) for which most measured bedload masses were smaller than 20 kg; for the Ruetz, 15 out of 21  
 160 calibration measurements also have bedload masses smaller than 20 kg. Using the  $k_{\text{tot}}$  coefficient from Eq. (3) in Eq. (1)  
 161 results in very similar statistical properties as compared to using  $k_{\text{lin}}$  in Eq. (1), also with a slightly poorer performance  
 162 (Table 3).

163 Systematic flume experiments were performed for different grain size classes to investigate the dependence of a linear  
 164 calibration coefficient, defined as  $k_{\text{bj}} = \text{IMP}/M$ , on grain size  $D$  (Wyss et al., 2016b). This study used bedload particles from  
 165 four streams including the Ruetz and Fischbach, and it was found that  $k_{\text{bj}}$  values showed a local maximum at a grain size  $D$   
 166 of around 40 mm, in agreement with earlier flume experiments using quartz spheres of different diameters (Rickenmann et  
 167 al., 2014). Therefore, we analysed the field calibration measurements from the Ruetz and Fischbach in a similar way (Fig. 6),  
 168 and these data essentially confirmed the findings from the flume experiments. The bedload samples from the Ruetz and  
 169 Fischbach show a general tendency for  $D_{84}$  to increase with increasing unit bedload transport rate  $q_b$  (Fig. 7), where  $D_{84}$  is  
 170 the grain size for which 84 % of material by weight are finer (determined for particles with  $D > 10$  mm). It is therefore not  
 171 surprising that  $k_{\text{bj}}$  values also exhibit a local maximum when plotted against the impulse rate,  $\text{IMPT}$  (Fig. 8), which is a  
 172 proxy for transport rate, and where  $\text{IMPT} = \text{IMP}/(T_s w_p)$ , with the plate width  $w_p = 0.5$  m. Finally this lead us to determine  
 173 alternative calibrations in terms of unit bedload transport rate per plate width  $q_{b,p}$  as a function of impulse rate,  $\text{IMPT}$  (Fig.  
 174 9), with a limiting value of around 0.5 to 1 ( $0.5^{-1} \text{ m}^{-1} \text{ s}^{-1}$ ) to separate the two ranges with a different power law function:

$$175 \quad q_{b,p} = a_1 \text{IMPT}^{b_1} \quad \text{for } \text{IMPT} < 0.48 \text{ (} 0.5^{-1} \text{ m}^{-1} \text{ s}^{-1} \text{)} \quad (4)$$

$$176 \quad q_{b,p} = a_2 \text{IMPT}^{b_2} \quad \text{for } \text{IMPT} > 0.48 \text{ (} 0.5^{-1} \text{ m}^{-1} \text{ s}^{-1} \text{)} \quad (5)$$

177 where the units for  $q_{b,p}$  are in ( $\text{kg } 0.5^{-1} \text{ m}^{-1} \text{ s}^{-1}$ ) and for  $\text{IMPT}$  in ( $0.5^{-1} \text{ m}^{-1} \text{ s}^{-1}$ ), and the coefficients and exponents are given in  
 178 Table 3. Here, we determined  $q_{b,p}$  and  $\text{IMPT}$  deliberately per unit width of one plate since using the traditional 1 m unit  
 179 width would result in different coefficients  $a_1$  and  $a_2$  (and a different threshold value  $\text{IMPT}$  separating the application range  
 180 of Eq. 4 and Eq. 5), which would entail the risk of erroneous transformations of measured  $\text{IMPT}$  values into  $q_{b,p}$  values for  
 181 each plate.

182 In Fig. 9, the regression relation for higher impulse rates was derived based on 14 calibration measurements from the  
 183 Fischbach with  $\text{IMPT} > 1$  [ $(1/0.5) \text{ m}^{-1} \text{ s}^{-1}$ ]. Similarly, the regression relation for lower impulse rates was derived based on 17  
 184 measurements from the Fischbach and 19 measurements from the Ruetz, all with  $\text{IMPT} < 1$  [ $(1/0.5) \text{ m}^{-1} \text{ s}^{-1}$ ]. The two power  
 185 law relations intersect at  $\text{IMPT} = 0.48$  [ $(1/0.5) \text{ m}^{-1} \text{ s}^{-1}$ ]. Using this limiting value, they were applied to the Fischbach and





186 Ruetz data, resulting in the statistical properties of the calibration relations (4) and (5) as reported in Table 3. It appears that  
187 the data from both channel sites can be described reasonably well with these calibrations relations, the relative standard  
188 deviation  $s_{e,r}$  being about 98% for the higher impulse rates and about 110% for the higher impulse rates (Table 3). If Eqs.  
189 (4) and (5) are applied to all calibration measurements of each stream separately, the clearly better statistical properties result  
190 for the Fischbach ( $r^2 = 0.97$ ,  $s_{e,r} = 61\%$ ) than for the Ruetz ( $r^2 = 0.50$ ,  $s_{e,r} = 145\%$ ). In comparison to the calibration relation  
191 determined with Eq. (2) for the Fischbach, Eqs. (4) and (5) will predict larger bedload transport rates for very small or very  
192 large *IMPT* values (Fig. 9).

### 193 3.2 Coarsening of grain sizes with increasing bedload flux reflected in geophone signal

194 The amplitude histograms (AH data) for each calibration measurement were used to estimate grain size distributions (GSD)  
195 for the basket sampler measurements, which were then compared with the sieve analyses of the bedload samples. For the  
196 analysis of the AH data, the lowest class with impulses for  $A_{\max} < 0.056$  V was excluded, as this class represents  
197 predominantly signal noise. For the remaining 16 classes the sum of the impulses per amplitude class was determined for all  
198 1 min time steps for the duration  $T_s$ . This resulted in the proportion of impulses per amplitude class per calibration  
199 measurement, not yet weighted for grain size. The impulses per class were weighted by the geometric mean diameter of each  
200 class (Table 2) to the 2<sup>nd</sup> power,  $D_m^2$ , to estimate the cumulative distribution of AH-values; this weighting procedure  
201 corresponds essentially to the method of Wyss et al. (2016), which is summarized in Appendix A. It is also noted that the  
202 start (and end) time of the bedload sampling does not exactly correspond to the start (and end) time of the recorded AH data,  
203 which introduced a further (generally minor) uncertainty when interpolating AH data for the first and last recording time step  
204 of each bedload sampling period. For the results shown in Figures 10 and 11, the GSD was averaged for given classes of unit  
205 bedload transport rates  $q_b$ , assigning the same weight to each measurement in a given  $q_b$  class. Bedload transport classes and  
206 corresponding abbreviation names are defined in Fig. 10 and 11.

207 For the bedload samples from both Fischbach and Ruetz a general coarsening trend of the grain size distribution (GSD)  
208 with increasing unit bedload transport rate  $q_b$  can be observed, in agreement with general bedload transport theory (Parker,  
209 2008). However, GSDs from individual calibration measurements are quite variable within given classes of  $q_b$ , both for the  
210 bedload samples and for the estimated GSD from the AH values, and do not necessarily follow the general trend. The GSDs  
211 estimated from the AH values generally show a qualitatively similar trend as the GSDs from the direct bedload samples, but  
212 with a limited quantitative agreement between the two methods.

213 For the Fischbach (Fig. 10) it is noted that only 2 calibration samples were available for the class Fi1, and these had the 2  
214 smallest bedload masses (with 19 and 8 kg, respectively); this may be a reason for the poor agreement between estimated  
215 and measured GSDs. Similarly, the largest  $q_b$  class Fi4 for the Fischbach includes only 1 bedload sample. For the Ruetz (Fig.  
216 11) we note that for the classes Ru1 and Ru3 the bedload masses were relatively small, including only 5 to 6 kg. Together  
217 with a small number of bedload samples (3 and 2, respectively), this may again be one reason for the relatively poor



218 agreement between estimated and measured GSDs. In contrast, the bedload masses for the Ruetz for the class Ru2 (11 to 23  
219 kg) and Ru4 (15 to 129 kg) were clearly larger.

### 220 3.3 Environmental noise pick-up of the geophone signal

221 Both measuring stations are situated at a relatively high elevation, and the stream catchments include mountain peaks with  
222 elevations above 3000 m a.s.l. Therefore the runoff during the winter period is very low, with a base flow below  $0.6 \text{ m}^3 \text{ s}^{-1}$  at  
223 the Fischbach and below  $0.3 \text{ m}^3 \text{ s}^{-1}$  at the Ruetz. During such flow conditions, only about half or two thirds of the sill with  
224 the steel plates is submerged under water (Fig. 2, Fig. S2). However, during winter geophone impulses are regularly  
225 recorded at all the geophone sensors in both streams (Fig. 12, Fig. 13). According to hydraulic calculations and observations  
226 the sill becomes fully submerged for flows of about  $2.5 \text{ m}^3 \text{ s}^{-1}$  at the Fischbach and about  $2.0 \text{ m}^3 \text{ s}^{-1}$  at the Ruetz. Therefore it  
227 is unlikely that these geophone impulses are the result of bedload transport.

228 For the Fischbach and the discharge classes smaller than  $3 \text{ m}^3 \text{ s}^{-1}$  the mean  $IMP_{15}$  values per 15 minutes ( $IMP_{15}$ ) vary  
229 between about 0.3 and 2.0. A similar analysis as in Fig. 12 but with a finer discharge resolution (classes of  $0.25 \text{ m}^3 \text{ s}^{-1}$ ) is  
230 presented in Fig. S3. It is also obvious that plates (sensors) no. 1 to 3 generally recorded more impulses than the other plates  
231 no. 4 to 8 (Fig. 12, Fig. S3), which is unlikely a result of bedload transport. For discharges up to about  $3 \text{ m}^3 \text{ s}^{-1}$  traffic noise  
232 appears to be a likely source of the geophone impulses, since the local road passes on the river right side very close to the  
233 plates no. 1 to 3 (Fig. 2). For discharge classes larger than  $4 \text{ m}^3 \text{ s}^{-1}$  the plates no. 4 to 8 (which have a larger water depth than  
234 plates no. 1 to 3) start to record more impulses on average ( $IMP_{15}$ ) than plates no. 1 to 3; in addition the  $IMP_{15}$  values start to  
235 increase with increasing discharge (Fig. 12, Fig. S3). This behaviour is more in line with expectations from bedload–  
236 transport induced signals.

237 For the Ruetz and the discharge classes smaller than  $1.0 \text{ m}^3 \text{ s}^{-1}$  the mean  $IMP_{15}$  values vary between about 0.2 and 2.0.  
238 Plates no. 5 to 8 generally recorded more impulses than the other plates no. 1 to 4 (Fig. 13, Fig. S4). The plates no. 1 to 3 are  
239 typically not submerged during these flow conditions, and no signal is to be expected from bedload transport. Again, traffic  
240 noise appears to be a likely source of the measured geophone impulses. The plates on the river left side (5 to 8) tend to  
241 register more impulses on average because the access road to the parking lot passes on this side, hence more parking traffic  
242 is to be expected. A clearer dominance of the plates no. 5 to 8 (which have a larger water depth than plates no. 1 to 4)  
243 becomes apparent for discharge classes larger than about  $1.5 \text{ m}^3 \text{ s}^{-1}$  at the Ruetz (Fig. 13, Fig. S4), which is in line with  
244 expectations from bedload–transport induced signals. The mean value of  $IMP_{15}$  averaged over all eight plates becomes larger  
245 than about 2 for discharges larger than roughly  $2.0 \text{ m}^3 \text{ s}^{-1}$ , and above this discharge level the  $IMP_{15}$  values start to increase in  
246 general with increasing discharge.

247 To further investigate the potential source of the implausible geophone recordings, we classified the measured  $IMP_{15}$   
248 values into 15 minute intervals during each day–time (Figs. S5, S6). For both streams and low flows, there is a clear daily  
249 cycle of geophone impulse activity although discharge remains rather constant during the entire day. This pattern clearly is  
250 present for the Fischbach for discharges  $Q$  smaller than about  $3 \text{ m}^3 \text{ s}^{-1}$  and for the Ruetz for  $Q$  smaller than about  $1.5 \text{ m}^3 \text{ s}^{-1}$ .





251 Geophone activity is higher during the afternoon and the first half of the night at the Fischbach, and primarily during day  
252 time at the Ruetz. A clear absence of this or a similar daily pattern is evident for the Fischbach for  $Q$  larger than about  $6 \text{ m}^3 \text{ s}^{-1}$   
253 <sup>1</sup> and for the Ruetz for  $Q$  larger than about  $3.5 \text{ m}^3 \text{ s}^{-1}$  (Fig. S5, S6). This is a further indication that the geophone impulses at  
254 smaller discharges are mainly traffic induced. Taken together, the above analysis and interpretation suggests that bedload  
255 transport may be the dominant source of producing geophone impulses above a critical discharge  $Q_c$  of about  $3.5 \text{ m}^3 \text{ s}^{-1}$  at the  
256 Fischbach, and above a  $Q_c$  of about  $1.5 \text{ m}^3 \text{ s}^{-1}$  at the Ruetz.

257 Turowski et al. (2011) analysed the start and end of bedload transport in gravel-bed streams, including geophone  
258 measurements from the Fischbach and Ruetz for the years 2008 and 2009. Based on the above delineation of the  $Q_c$  values  
259 for the two streams, it is estimated that they used about 62 % (out of 95 measurements) potentially implausible values for the  
260 Fischbach and about 41 % (out of 492 measurements) potentially implausible values for the Ruetz. If these values were  
261 discarded from their analysis, this would change the histograms of the discharge at the start and end of transport for the two  
262 streams but it would not affect the general conclusions of the study.

## 263 4. Discussion

### 264 4.1 Calibration relations for the Swiss plate geophone system and grain size determination

265 For a system such as the Swiss plate geophone it is known that the signal response depends on factors such as grain size,  
266 fluid or particle velocity, particle shape and mode of transport (i.e. sliding, rolling, saltating), and impact angle and impact  
267 location on the steel plate (e.g. Wyss et al., 2016b; Rickenmann, 2017b). For a given stream we may assume that the most of  
268 these factors vary within a given range, and the linear calibration coefficients primarily vary with flow conditions. Therefore,  
269 we expect that the mean signal response from a given particle size traveling over the plate becomes more stable the larger is  
270 the total number of particles that have been transported over the plate. This is the main reason why we have primarily  
271 considered the summed geophone summary values in the past (e.g. Rickenmann et al., 2012, 2014). Calibration  
272 measurements from various sites confirmed the expectation that random factors influencing the signal response tend to be  
273 more averaged out for longer integration periods (Rickenmann and McArdell, 2007, 2008; Rickenmann et al., 2012, 2014;  
274 Wyss et al., 2016a, 2016c).

275 However, it may also be interesting to consider calibration relations for example between bedload rates and impulse  
276 rates. If a linear calibration relation in the form of Eq. (1) is generally valid, a division of  $M$  and  $IMP$  by the sampling  
277 duration  $T_s$  to determine rates will typically result in similar values for the linear calibration coefficient. Having performed  
278 this alternative analysis in terms of bedload rates and impulse rates for the data of this study, two distinctly different ranges  
279 of geophone signal response were found based on the data from the Fischbach (Fig. 9). These calibration measurements  
280 suggest that two power law calibration relations in terms of rates provide a better fit than a single linear calibration relation  
281 for the entire domain. The existence of two different ranges is likely a result of a changing GSD with increasing bedload  
282 transport rates. We therefore also plotted data from calibration measurements at many other sites (Fig. 14), but no clear trend



283 for a similar pattern can be observed for most of these sites. The only exception is the Urslau stream in Austria; the  
284 individual calibration measurements for this stream indicate a trend for a power law relation between  $q_b$  and  $IMPT$  with an  
285 exponent  $b < 1$  for smaller  $q_b$  values and with an exponent  $b > 1$  for larger  $q_b$  values (Kreisler et al., 2016). These calibration  
286 measurements cover a range of about three orders of magnitude of  $q_b$  values; however different methods were used to obtain  
287 the bedload samples for smaller and larger bedload transport intensities, and for the smaller range of  $q_b$  values the number of  
288 measurements is limited.

289 We used the AH data recorded during the calibration measurements at the Fischbach and Ruetz to estimate the  
290 transported bedload mass for each calibration measurement,  $M_{est}$ , by applying the procedure presented by Wyss et al.  
291 (2016a). This method is summarized in Appendix A, and it was specifically developed for the measuring conditions at the  
292 Erlenbach stream in Switzerland. Here, we used Eq. (A3) with the coefficient and exponent determined from the Erlenbach  
293 measurements; the relation of Eq. (A3) is expected to vary somewhat from site to site, and its application here is therefore  
294 associated with uncertainty. To assess the performance of this procedure when applied to the Fischbach and Ruetz, we  
295 plotted the ratio of estimated to observed bedload mass,  $M_{est}/M$ , as a function of bedload transport rate per plate  $q_{b,p}$  and of  
296 observed mass  $M$  (Fig. 15). There is generally an over-estimation of bedload mass, up to a factor of about 10. Interestingly,  
297 the over-estimation decreases with increasing bedload transport rate (Fig. 15a). This result is in agreement with Fig. 14,  
298 which suggests that site-specific differences for calibration relations in terms of bedload transport rates and impulse rates  
299 tend to be relatively smaller for higher values of  $q_b$ . The degree of over-estimation of bedload mass as well as the scatter  
300 around a mean trend line for both streams appears to decrease also with increasing bedload mass for the data of the  
301 Fischbach and Ruetz (Fig. 15b), but this trend is somewhat less pronounced. Concerning grain size estimation from bedload  
302 surrogate measuring techniques, it may be noted that only a few other acoustic measuring techniques were (partly) successful  
303 in determining bedload transport by grain size classes from field measurements (Barrière et al., 2015b, using an impact plate  
304 hydrophone system; Mao et al., 2016, using a Japanese impact pipe microphone system).

305 To illustrate the uncertainty associated with using different calibration relations, we determined the yearly bedload ( $YBL$ )  
306 for 2010, which represents the year with the largest peak discharges and the largest  $YBL$  values (Table 4) for the period  
307 2008–2013. For both streams, the  $YBL$  values are larger when using Eqs. (4) and (5) as compared to using Eq. (1); this is not  
308 surprising when comparing the linear with the power law calibration relations in Fig. 9. The power law calibration relations  
309 result in a 66 % higher  $YBL$  for the Fischbach and in a 85 % higher  $YBL$  for the Ruetz, if only plausible  $IMP$  values for  
310 discharges larger than  $Q_c$  are considered; the differences are larger if the entire  $IMP$  data set for 2010 is considered,  
311 including many implausible values recorded during low flow periods (Table 4). The between-stream comparison shows a  
312 much larger  $YBL$  for the Fischbach than for the Ruetz, which is due to more frequent peak discharges in the Fischbach  
313 exceeding about  $10 \text{ m}^3 \text{ s}^{-1}$  during the year 2010 (Fig. S7, S8).



#### 314 4.2 Environmental noise pick-up of the geophone signal

315 Hydrophones (underwater microphones) have been used to monitor bedload transport both in riverine and in coastal  
316 environments (e.g. Thorne, 1990; Camenen et al. 2012; Basset et al., 2013). The objective of using such a system is to record  
317 self-generated noise produced by collisions of moving bedload particles against each other or against the bed. The  
318 application of this bedload surrogate measuring system can be impaired by other sources of noise, which may be caused by  
319 vessel traffic, marine seismic exploration, or underwater military operations. If the main interest is in the acoustic signal due  
320 to bedload transport, discounting for other sources of noise may be challenging and will also depend for example on the  
321 spatial distance and the dominant frequencies of the different acoustic sources (Hildebrand, 2009; Etter, 2012; Basset et al.,  
322 2013).

323 For the application of impact plates with acoustic sensors installed in a streambed there is very few experience with non-  
324 bedload transport related sources of noise that may compromise their usefulness. We have shown in section 3.3 that road  
325 traffic is a likely source of environmental noise producing a similarly strong signal at the SPG system as low-intensity  
326 bedload transport during periods with moderate discharges. This observation was made for our two study streams Fischbach  
327 and Ruetz, where in both cases the stream bed runs very close-by to roads, which are located only about half the stream-  
328 width away from the edge of the bed. We have checked the impulse counts recorded for SPG systems installed at mountain  
329 streams in Switzerland, particularly for low flow periods during winter time. There were generally very few impulses  
330 recorded at these sites, indicating that road traffic is not an important source of noise. At these sites roads with regular traffic  
331 are situated clearly farther away from the channel profile than at the two Austrian sites of this study: at the Navisence stream  
332 in Zinal (Ancy et al., 2015) about 45 m (or 3 times the stream width), at the Albula River in Tiefencastel (Rickenmann et  
333 al., accepted) about 30 m (or twice the stream width) to a road or about 15 m to a parking lot of a single building, and at the  
334 Avançon de Nant stream near Pont de Nant about 20 m (or 4 times the stream width). The SPG system at the Erlenbach  
335 stream in Switzerland (Rickenmann et al., 2012) is situated about 45 m away from a road; at this site we observed  
336 implausible impulse counts limited to very short time periods that were likely due to hikers or possibly game passing at the  
337 site.

338 At the Riedbach stream in Switzerland the geophone measuring site is situated at a water intake at an elevation of 1800 m  
339 a.s.l, with few direct sunshine and often freezing temperatures during winter time. The access road ends at the water intake  
340 and is not open to the public. For a seven year period from 2009 to 2015 geophone measurements showed no systematic  
341 relationship between *IMP* and *Q* for discharges *Q* smaller than about  $0.4 \text{ m}^3 \text{ s}^{-1}$ , but a considerable number of *IMP* were  
342 recorded for *Q* values as small as  $0.05 \text{ m}^3 \text{ s}^{-1}$  (Schneider et al., 2016). These discharge conditions are typical for the winter  
343 period, and it was hypothesized that ice transport or break-up may be mainly responsible for the impulse counts. Impulses  
344 may be typically as high as between 1 and 100 impulses for all seven plates and for 10 minute recording intervals.  
345 Calculating a mean impulse value per plate for  $Q < 0.3 \text{ m}^3 \text{ s}^{-1}$  and including also zero values, this results in an average



346 duration of about 5 hours for one impulse to be registered at the Riedbach by one of the seven steel plates. This relatively  
347 low occurrence frequency does not contradict the ice transport or break-up hypothesis.

## 348 5. Conclusions

349 The Fischbach and Ruetz gravel-bed streams are characterized by important runoff and bedload transport during the  
350 snowmelt season. As a bedload surrogate measuring technique, the Swiss plate geophone (SPG) system has been installed in  
351 2007 in both streams. During the six year period 2008 – 2013, 31(Fischbach) and 21 (Ruetz) direct bedload samples were  
352 obtained in the two streams, and these measurements were analysed to obtain calibration relations for the SPG system at the  
353 two sites.

354 As applied at many other SPG sites in the past, we first established calibration relations using total transported bedload  
355 mass and the number of geophone impulses. A second way of analysing the geophone calibration measurements consisted in  
356 using bedload transport rates and geophone impulse rates. For the Fischbach the second approach resulted in two power law  
357 calibration relations, with different coefficients and exponents for small and large transport rates. The exponent was smaller  
358 than one for small transport rates, and larger than one for larger transport rates. For the Ruetz data with essentially only  
359 lower transport intensities, the power law relation derived from the Fischbach is also in reasonable agreement with the Ruetz  
360 calibration measurements. The non-linear power law calibration relations are in qualitative agreement with the observed  
361 coarsening of the bedload with increasing transport rates. According to findings from flume studies the signal response per  
362 unit bedload mass increases for small grains up to grain size of approximately 40 mm, and decreases again for larger grains  
363 with increasing particle size (Wyss et al., 2016b); this provides qualitative support for the existence of the two power law  
364 relations. A similar behaviour could be observed only for the calibration measurements at the Urslau stream in Austria  
365 (Kreisler et al., 2016). In contrast, calibration measurements from six other sites, including the Ruetz stream, do not show  
366 evidence for the existence of similar two-range power law calibration relations.

367 Amplitude information from the geophone signal was recorded in minute intervals at the Fischbach and Ruetz by  
368 summing impulse counts separately for different amplitude classes (so-called AH data). Since signal amplitude correlates  
369 with grain size at several SPG sites (Wyss et al., 2016a, 2016b, 2016c), this information was used to estimate the grain size  
370 distribution for the bedload samples from the Fischbach and Ruetz. It was found that the observed coarsening of the grain  
371 size distribution with increasing bedload flux could be qualitatively reproduced from the geophone signal using the AH data.

372 For smaller discharges at the Fischbach and Ruetz, in particular during the winter time, it was found that many  
373 implausible geophone impulse counts were recorded. Both SPG measuring sites are situated very close to local roads with  
374 regular traffic. The roads are only about half the stream width away from the steel plates, and we therefore identified vehicle  
375 traffic as a likely source for the implausible geophone impulses. This is indirectly supported by a comparison with other SPG  
376 sites in Switzerland. At most of these sites only very few implausible geophone impulse counts were recorded in the past,



377 which is probably due to the fact that the local roads are farther away from the steel plates, generally at least once or twice  
378 the stream width.

## 379 6. Data availability

380 The data cannot be made publicly available for the time being since it is used by the Hydropower Company TIWAG, the  
381 owner and provider of the data, in an ongoing hydropower project authorisation procedure.

## 382 7. Appendix A: Summary of the amplitude histogram method of Wyss et al. (2016a)

383 Information about the grain–size distribution of the transported bedload over a Swiss geophone plate can be determined  
384 using the number of impulses per amplitude class (called amplitude histogram method). Amplitude histograms (AH data)  
385 can be interpreted as a statistical distribution of the signal’s amplitude over a given time interval. Using the number of  
386 bedload particles per unit mass, absolute bedload masses for each grain–size class were calculated for the Erlenbach stream  
387 in Switzerland.

388 For  $j$  grain size classes an amplitude threshold value  $A_{th}$  (upper class boundary value, in V) corresponds to a threshold  
389 particle size  $D$  in (mm) separating the grain size class (Wyss et al. 2016a). In this study an empirical relation given in Wyss  
390 et al. (2016c) was used (see also Table 2):

$$391 \quad D = 85.5 A_{th}^{0.41} \quad (A1)$$

392 Wyss et al. (2016a) assumed that the number of impulses per amplitude class,  $IMP_j$ , are related to the number of particles in  
393 the corresponding grain size class,  $N_j$ , with a mean weight,  $G_{mj}$ , by a coefficient  $\alpha_j$  determined from the bedload samples, as  
394 follows:

$$395 \quad IMP_j = \alpha_j N_j \quad (A2)$$

396 For the calibration of the method for the Erlenbach 31 bedload samples were used. The analysis resulted in the following  
397 empirical power law relation between  $\alpha_j$  and the class mean grain size  $D_{mj}$  in [mm] where the median value of  $\alpha_j$  of all  
398 bedload samples was used to determine the empirical relation (A3):

$$399 \quad \alpha_j = 0.0093 D_{mj}^{1.09} \quad (A3)$$

400 where the coefficient 0.0093 has the units [ $\text{mm}^{-1.09}$ ]. Finally, to estimate the bedload mass per grain size class, the following  
401 relation can be used:

$$402 \quad M_{est} = N_j G_{mj} = \frac{IMP_j G_{mj}}{\alpha_j} \quad (A4)$$



403 The above procedure was used to estimate the bedload mass for each calibration sample from the Fischbach and the Ruetz,  
404 as reported in section 4.1 in the Discussion. To determine the mean weight,  $G_{mj}$  in [g] for each grain size class with  $D_{mj}$  in  
405 [mm], the following empirical relations were used, based on investigations reported in Wyss et al. (2016c):

$$406 \quad G_{mj} = 0.00165 D_{mj}^{2.94} \quad \text{for the Fischbach} \quad (A5)$$

$$407 \quad G_{mj} = 0.00111 D_{mj}^{3.03} \quad \text{for the Ruetz} \quad (A6)$$

408 Considering Eqs. (A5) or (A6) together with Eqs. (A2) and (A3) it follows that the number of grains per class is  
409 approximately proportional to  $IMP_j \bullet D_{mj}^2$ . We used this proportionality in section 3.2 to estimate the GSD for the calibration  
410 measurements from the Fischbach and Ruetz based on the recorded AH data. The main uncertainty in transferring the  
411 method of Wyss et al. (2016a) determined for the Erlenbach to another site is the use of Eq. (A3) which may differ at  
412 other sites. We used the entire procedure reported here, including Eq. (A3) with the coefficient and exponent determined  
413 from the Erlenbach measurements, in section 4.1 to explicitly estimate the total bedload mass for each calibration  
414 measurement from the Fischbach and Ruetz based on the recorded AH data.

## 415 8. Supplement link

416 → see also Supplementary Material

## 417 9. Author contribution

418 BF was the main responsible for the concept and installation of the SPG system at the Fischbach and Ruetz. He had  
419 suggested to record the AH data as a memory efficient way to extract grain-size relevant information from the raw geophone  
420 signal. DR was responsible for the analysis and wrote the paper. Support of colleagues for figure preparation is  
421 acknowledged below.

422

## 423 10. Acknowledgements

424 We are grateful to the Tyrolean Hydropower Company (TIWAG) for having performed the geophone calibration  
425 measurements in the Fischbach and Ruetz streams and for having provided these data and the continuous geophone  
426 measurements to WSL for further analysis. The study was supported by SNF grants 200021\_124634 and 200021\_137681.  
427 We thank Nicloas Steeb, Philipp von Arx, and Thomas Weninger for help with the preparation of some figures; TW also  
428 performed grain size analyses of the streambed surface.

429





430 **11. References**

431

- 432 Ancey, C., Bohorquez, P., and Bardou, E.: Sediment transport in mountain rivers, *ERCOFTAC Bulletin*, 100, 37–52, 2015.
- 433 Bänziger, R., and Burch, H.: Acoustic sensors as indicators for bed load transport in a mountain torrent, in: *Hydrology in*  
434 *Mountainous Regions I*, IAHS. Publ. no. 193, pp. 207–214, 1990.
- 435 Barrière, J., Krein, A., Oth, A., and Schenkluhn, R.: An advanced signal processing technique for deriving grain size  
436 information of bedload transport from impact plate vibration measurements, *Earth Surf. Proc. Land.*, 40, 913–924, 2015a.
- 437 Barrière, J., Oth, A., Hostache, R., and Krein, A.: Bed load transport monitoring using seismic observations in a low-  
438 gradient rural gravel bed stream, *Geophys. Res. Lett.*, 42, 2294–2301, 2015b.
- 439 Barton, J. S., Slingerland, R. L., Pittman, S., and Gabrielson, T. B.: Monitoring coarse bedload transport with passive  
440 acoustic instrumentation: A field study, in: *U.S. Geological Survey Scientific Investigations Report 2010–5091*, 38–51,  
441 available at: <https://pubs.usgs.gov/sir/2010/5091/papers/listofpapers.html>, 2010.
- 442 Bassett, C., Thomson, J., and Polagye, B.: Sediment-generated noise and bed stress in a tidal channel, *J. Geophys. Res.*  
443 *Oceans*, 118, 2249–2265, 2013.
- 444 Bathurst, J. C., Graf, W. H., and Cao, H. H.: Bed load discharge equations for steep mountain rivers, in: *Sediment transport*  
445 *in gravel-bed rivers*, Wiley & Sons, New York, USA, 453–477, 1987.
- 446 Beylich, A. A., and Laute, K.: Combining impact sensor field and laboratory flume measurements with other techniques for  
447 studying fluvial bedload transport in steep mountain streams, *Geomorphology*, 218, 72–87, 2014.
- 448 Camenen, B., Jaballah, M., Geay, T., Belleudy, P., Laronne, J. B., and Laskowski, J. P.: Tentative measurements of bedload  
449 transport in an energetic alpine gravel bed river, in: *River Flow 2012*, Taylor & Francis Group, London, 379–386, 2012.
- 450 Gomez, B.: Bedload transport, *Earth–Sci. Rev.*, 31, 89–132, 1991.
- 451 Goto, K., Itoh, T., Nagayama, T., Kasai, M., and Marutani, T.: Experimental and theoretical tools for estimating bedload  
452 transport using a Japanese pipe hydrophone, *Int. J. Erosion Control Engineering*, 7(4), 101–110, 2014.
- 453 Gray, J. R., Laronne, J. B., and Marr, J. D. G.: Bedload-surrogate Monitoring Technologies, U.S. Geological Survey  
454 Scientific Investigations Report 2010–5091, 37p., available at: <http://pubs.usgs.gov/sir/2010/5091/>, 2010.
- 455 Habersack, H., Kreisler, A., Rindler, R., Aigner, J., Seitz, H., Liedermann, M., and Laronne, J. B.: Integrated automatic and  
456 continuous bedload transport monitoring in gravel bed rivers, *Geomorphology*, doi:10.1016/j.geomorph.2016.10.020,  
457 2016.
- 458 Hegg, C., McArdell, B. W., Badoux, A.: One hundred years of mountain hydrology in Switzerland by the WSL, *Hydrol.*  
459 *Process.*, 20, 371–376, 2006.
- 460 Krein, A., Klinck, H., Eiden, M., Symader, W., Bierl, R., Hoffmann, L., and Pfister, L.: Investigating the transport dynamics  
461 and the properties of bedload material with a hydro-acoustic measuring system, *Earth Surf. Proc. Land.*, 33, 152–163,  
462 2008.



- 463 Kreisler, A., Moser, M., Aigner, J., Rindler, R., Tritthard, M., Habersack, H.: Analysis and classification of bedload transport  
464 events with variable process characteristics, *Geomorphology*, doi:10.1016/j.geomorph.2016.06.033, 2016.
- 465 Leopold, L. B., Emmett, W. W.: Bedload and river hydraulics – Inferences from the East Fork River, Wyoming, U.S.  
466 Geological Survey Professional Paper 1583, 1997.
- 467 Mao, L., Carrillo, R., Escauriaza, C., and Iroume, A.: Flume and field-based calibration of surrogate sensors for monitoring  
468 bedload transport, *Geomorphology*, 253, 10–21, 2016.
- 469 Mizuyama, T., Oda, A., Laronne, J. B., Nonaka, M., and Matsuoka, M.: Laboratory tests of a Japanese pipe geophone for  
470 continuous acoustic monitoring of coarse bedload, in: U.S. Geological Survey Scientific Investigations Report 2010–  
471 5091, 319–335, available at: <https://pubs.usgs.gov/sir/2010/5091/papers/listofpapers.html>, 2010a.
- 472 Mizuyama, T., Laronne, J. B., Nonaka, M., Sawada, T., Satofuka, Y., Matsuoka, M. et al.: Calibration of a passive acoustic  
473 bedload monitoring system in Japanese mountain rivers, in: U.S. Geological Survey Scientific Investigations Report  
474 2010–5091, 296–318, available at: <https://pubs.usgs.gov/sir/2010/5091/papers/listofpapers.html>, 2010b.
- 475 Møen, K. M., Bogen, J., Zuta, J. F., Ade, P. K., and Esbensen, K. Bedload measurement in rivers using passive acoustic  
476 sensors, in: U.S. Geological Survey Scientific Investigations Report 2010–5091, 336–351, available at:  
477 <https://pubs.usgs.gov/sir/2010/5091/papers/listofpapers.html>, 2010.
- 478 Nitsche, M., Rickenmann, D., Turowski, J. M., Badoux, A., Kirchner, J. W.: Evaluation of bedload transport predictions  
479 using flow resistance equations to account for macro-roughness in steep mountain streams, *Water Resour. Res.*, 47,  
480 W08513, doi:10.1029/2011WR010645, 2011.
- 481 Recking, A.: A comparison between flume and field bed load transport data and consequences for surface based bed load  
482 transport prediction, *Water Resour. Res.*, 46, W03518, doi:10.1029/2009WR008007, 2010.
- 483 Reid, S. C., Lane, S. N., and Berney, J. M.: The timing and magnitude of coarse sediment transport events within an upland  
484 gravel-bed river, *Geomorphology*, 83, 152–182, 2007.
- 485 Rickenmann, D.: Sediment load and discharge in the Erlenbach Stream, in: *Dynamics and Geomorphology of Mountain  
486 Rivers*, Lecture Notes in Earth Sciences, 52, 53–66, 1994.
- 487 Rickenmann, D.: Sediment transport in Swiss torrents, *Earth Surf. Proc. Land.*, 22, 937–951, 1997.
- 488 Rickenmann, D.: Bedload transport measurements with geophones, hydrophones and underwater microphones (passive  
489 acoustic methods), in: *Gravel Bed Rivers and Disasters*, Wiley & Sons, Chichester, UK, 185–208, 2017a.
- 490 Rickenmann, D.: Bedload transport measurements with geophones and other passive acoustic methods, *J. Hydraul. Eng.–  
491 ASCE*, in press, 2017b.
- 492 Rickenmann, D., Antoniazza, G., Wyss, C. R., Fritschi, B., Boss., S.: Bedload transport monitoring with acoustic sensors in  
493 the Swiss Albula mountain river, *Proc. Int. Ass. Hydr. Sci.*, accepted.
- 494 Rickenmann, D., and McArdeall, B. W.: Continuous measurement of sediment transport in the Erlenbach stream using  
495 piezoelectric bedload impact sensors, *Earth Surf. Proc. Land.*, 32, 1362–1378, 2007.



- 496 Rickenmann, D., and McArdell, B. W.: Calibration measurements with piezoelectric bedload impact sensors in the Pitzbach  
497 mountain stream, *Geodin. Acta*, 21, 35–52, 2008.
- 498 Rickenmann, D., and Fritschi, B.: Bedload transport measurements using piezoelectric impact sensors and geophones, in:  
499 U.S. Geological Survey Scientific Investigations Report 2010–5091, 407–423, available at:  
500 <https://pubs.usgs.gov/sir/2010/5091/papers/listofpapers.html>, 2010.
- 501 Rickenmann, D., Turowski, J. M., Fritschi, B., Klaiber, A., and Ludwig, A.: Bedload transport measurements at the  
502 Erlenbach stream with geophones and automated basket samplers, *Earth Surf. Proc. Land.*, 37, 1000–1011, 2012.
- 503 Rickenmann, D., Turowski, J. M., Fritschi, B., Wyss, C., Laronne, J. B., Barzilai, R. et al.: Bedload transport measurements  
504 with impact plate geophones: comparison of sensor calibration in different gravel–bed streams, *Earth Surf. Proc. Land.*,  
505 39, 928–942, 2014.
- 506 Rigby, J. R., Kuhnle, R. A., Goodwiller, B. T., Nichols, M. H., Carpenter, W. O., Wren, D. G., and Chambers, J. P.:  
507 Sediment–generated noise (SGN): Comparison with physical bed load measurements in a small semi–arid watershed,  
508 Paper presented at the 2015 SEDHYD Conference, 19–23 April 2015, Reno, Nevada, USA, available at:  
509 <http://www.sedhyd.org/2015/>, 2015
- 510 Ryan, S. E., Dixon, M. K.: Spatial and temporal variability in stream sediment loads using examples from the Gros Ventre  
511 Range, Wyoming, USA, in: *Gravel–Bed Rivers VI: From Process Understanding to River Restoration*, in: *Developments*  
512 *in Earth Surface Processes*, 11, 387–407, 2008.
- 513 Schneider, J. M., Rickenmann, D., Turowski, J. M., Bunte, K., and Kirchner, J. W.: Applicability of bed load transport  
514 models for mixed–size sediments in steep streams considering macro–roughness, *Water Resour. Res.*, 51, 5260–5283,  
515 doi:10.1002/2014WR016417, 2015.
- 516 Schneider, J. M., Rickenmann, D., Turowski, J. M., Schmid, B., Kirchner, J. W.: Bed load transport in a very steep mountain  
517 stream (Riedbach, Switzerland): Measurement and prediction, *Water Resour. Res.*, 52, doi:10.1002/2016WR019308,  
518 2016.
- 519 Thorne, P. D.: The measurement of acoustic noise generated by moving artificial sediments, *J. Acoustic Soc. America*, 78,  
520 1013–1023, 1985.
- 521 Thorne, P. D.: Laboratory and marine measurements on the acoustic detection of sediment transport, *J. Acoustic Soc.*  
522 *America*, 80, 899–910, 1986.
- 523 Thorne, P. D.: Seabed generation of ambient noise, *J. Acoustic Soc. America*, 87, 149–153, 1990.
- 524 Tsakiris, A. G., Papanicolaou, A. N., and Lauth, T. J.: Signature of bedload particle transport mode in the acoustic signal of a  
525 geophone, *J. Hydraul. Res.*, 52(2), 185–204, 2014.
- 526 Turowski, J. M., Badoux, A., and Rickenmann, D.: Start and end of bedload transport in gravel–bed streams, *Geophys. Res.*  
527 *Let.*, 38, L04401, doi:10.1029/2010GL046558, 2011.



- 528 Uchida, T., Okamoto, A., Hayashi, S., Suzuki, T., Fukumoto, A., Yamashita, A., and Tagata, S.: Hydrophone observations of  
529 bedload transport in mountainous rivers of Japan, in: *Advances in River Sediment Research*, Taylor & Francis Group,  
530 London, 1749–1796, 2013.
- 531 Voulgaris, G., Wilkin, M. P., and Collins, M. B.: The in situ passive acoustic measurement of shingle movement under  
532 waves and currents: instrument (TOSCA) development and preliminary results, *Cont. Shelf Res.*, 15, 1195–1211, 1995.
- 533 Wyss, C. R., Rickenmann, D., Fritschi, B., Turowski, J. M., Weitbrecht, V., Boes, R. M.: Measuring bedload transport rates  
534 by grain-size fraction using the Swiss plate geophone signal at the Erlenbach, *J. Hydraul. Eng.–ASCE*, 142(5),  
535 04016003, doi: 10.1061/(ASCE)HY.1943-7900.0001090, 2016a.
- 536 Wyss, C. R., Rickenmann, D., Fritschi, B., Turowski, J. M., Weitbrecht, V., Boes, R. M.: Laboratory flume experiments with  
537 the Swiss plate geophone bedload monitoring system. Part I: Impulse counts and particle size identification, *Water*  
538 *Resour. Res.*, 52, 7744–7759, doi:10.1002/2015WR018555, 2016b.
- 539 Wyss, C. R., Rickenmann, D., Fritschi, B., Turowski, J. M., Weitbrecht, V., Travaglini, E., Bardou, E., Boes, R. M.:  
540 Laboratory flume experiments with the Swiss plate geophone bedload monitoring system. Part II: Application to field  
541 sites with direct bedload samples, *Water Resour. Res.*, 52, 7760–7778, doi:10.1002/2016WR019283, 2016c.
- 542
- 543



544

545 **Table 1.** Catchment and channel characteristics at the field sites and range of typical parameters for the conditions during the  
 546 geophone calibration measurements. The  $q_b$  values refer to bedload with  $D > 10$  mm.  
 547

	Fischbach	Ruetz
<i>Catchment parameters</i>		
Drainage area (km <sup>2</sup> )	71	28
Maximum elevation (m)	3497	3474
Site elevation (m)	1540	1684
Mean annual precipitation (mm)	1670	1880
% glacier	16	20
<i>Channel parameters (measuring site)</i>		
Gradient over 60 m upstream of geophone site S	1.7	2.5
Stream bed width (m)	8.5	8.5
Bed surface D <sub>84</sub> (m)	0.26	0.28
Bed surface D <sub>50</sub> (m)	0.09	0.10
<i>Parameter range for calibration periods</i>		
Period of calibration measurements used in this	2008–2013	2008–2013
No. of calibration measurements used in this study	31	21
Max. unit discharge $q_{\max}$ (m <sup>2</sup> /s)	1.97	0.97
Min. unit discharge $q_{\min}$ (m <sup>2</sup> /s)	0.56	0.41
Max. mean flow velocity $V_{\max}$ (m/s)	2.79	1.88
Min. mean flow velocity $V_{\min}$ (m/s)	1.51	1.02
Max. unit bedload transport rate, $q_{b,\max}$ (kg/sm)	7.20	0.214
Min. unit bedload transport rate, $q_{b,\min}$ (kg/sm)	0.0050	0.0025
Bedload samples: max. $D_{\max}$ (m)	0.350	0.150
Bedload samples: min. $D_{\max}$ (m)	0.030	0.050
Bedload samples: max. weight ( $D > 10$ mm) [kg]	431	128
Bedload samples: mean weight ( $D > 10$ mm) [kg]	70.0	20.6
Sampling duration of calibration measurements [s]	30 – 3600	600 – 3600
Recording interval of geophone summary values	900	900

548

549



550

551 **Table 2.** Threshold values of the signal amplitude  $A$  used for the impulse count of the amplitude histograms at the Fischbach  
552 and Ruetz. To estimate a corresponding particle size  $D$ , an empirical relation from Wyss et al. (2016c) was used.  
553  $D_{\text{mg}}$  is the geometric mean size of each particle class.  
554

$A_{\text{th}}$ [V]	0.056	0.079	0.112	0.158	0.224	0.316	0.447	0.631	0.891	1.259	1.778	2.512	3.548	5.012	7.079	10.0	12.0
$D$ [mm]	26.2	30.2	34.8	40.1	46.3	53.3	61.5	70.8	81.5	94.0	108	125	144	166	191	220	237
$D_{\text{mg}}$ [mm]		28.1	32.4	37.4	43.1	49.7	57.2	66.0	76.0	87.5	101	116	134	154	178	205	228

555

556





557

558 **Table 3.** Coefficients, exponents and statistical properties for the calibration relations according to eq. 1, 2, 3, 4, 5. All  
 559 calibration relations refer to bedload mass with  $D > 10$  mm, or unit bedload transport rate  $q_{b,p}$  for  $D > 10$  mm. In  
 560 the equations, the units are:  $M$  in [kg],  $q_{b,p}$  in [kg/0.5m/s] and  $IMPT$  in [1/0.5m/s]. Here  $r^2$  is the correlation  
 561 coefficient between values calculated with the regression relation and the recorded bedload masses. Similarly, in  
 562 all figures,  $r^2$  is determined between the predicted  $y$ -value and the observed  $y$ -value (in the linear domain). The  
 563 relative standard deviation  $s_{e,r}$  is determined for the ratios ( $M_{est}/M$ ) of estimated bedload mass  $M_{est}$  calculated with  
 564 the regression relation and the recorded impulses  $IMP$ , divided by the recorded bedload mass  $M$ . For the first three  
 565 relations, the number of calibration measurements ( $n$ ) are given in Table1, for the other two relations they are  
 566 listed in this table.  
 567

	Fischbach	Ruetz	both streams
$M = k_{lin} IMP$			
$k_{lin}$	0.0508	0.0436	
$r^2$	0.964	0.597	
significance level: probability p	<0.0001	<0.0001	
$s_{e,r}$	0.67	1.38	
$M = k_{pow} M^e$			
$k_{pow}$	0.134	1.40	
$e$	0.88	0.42	
$r^2$	0.967	0.576	
significance level: probability p	<0.0001	<0.0019	
$s_{e,r}$	0.78	0.92	
$M = k_{tot} IMP$			
$k_{tot}$	0.0558	0.0547	
$r^2$	0.964	0.597	
significance level: probability p	<0.0001	<0.0001	
$s_{e,r}$	0.73	1.73	
$q_{b,p} = a_1 IMPT^{b_1}$ for $IMPT < 0.48$ [1/0.5m/s]			
$a_1$	0.0237	0.0237	0.0237
$b_1$	0.48	0.48	0.48
$n$	15	15	30
$r^2$	0.559	0.790	0.524
significance level: probability p	<0.0001	<0.054	<0.0001
$s_{e,r}$	0.77	1.13	0.98
$q_{b,p} = a_2 IMPT^{b_2}$ for $IMPT > 0.48$ [1/0.5m/s]			
$a_2$	0.0436	0.0436	0.0436
$b_2$	1.29	1.29	1.29
$n$	16	6	22
$r^2$	0.964	0.517	0.966
significance level: probability p	<0.0001	<0.0001	<0.0001
$s_{e,r}$	0.37	1.71	1.11



568

569 **Table 4.** Comparison of yearly bedload (*YBL*, in t) calculated with two different calibration relations, for the year 2010 and  
 570 for different ranges of *Q* values. The *YBL* values represent transport over the entire stream width; as only every  
 571 second steel plate is equipped with a geophone sensor, the loads inferred from the geophone impulses were  
 572 multiplied by a factor of 2 in this table.  
 573

Stream	Year	Q range	Yearly bedload YBL-A (t) Eqs. (4,5)	Yearly bedload YBL-B (t) Eq. (1)	YBL-A / YBL-B
Fischbach	2010	all Q (including im- plausible IMP values)	10,800	6,430	1.68
		Q > 3.5 m <sup>3</sup> s <sup>-1</sup>	10,600	6,410	1.66
Ruetz	2010	all Q (including im- plausible IMP values)	1,360	621	2.19
		Q > 1.5 m <sup>3</sup> s <sup>-1</sup>	1,110	600	1.85

574

575

576

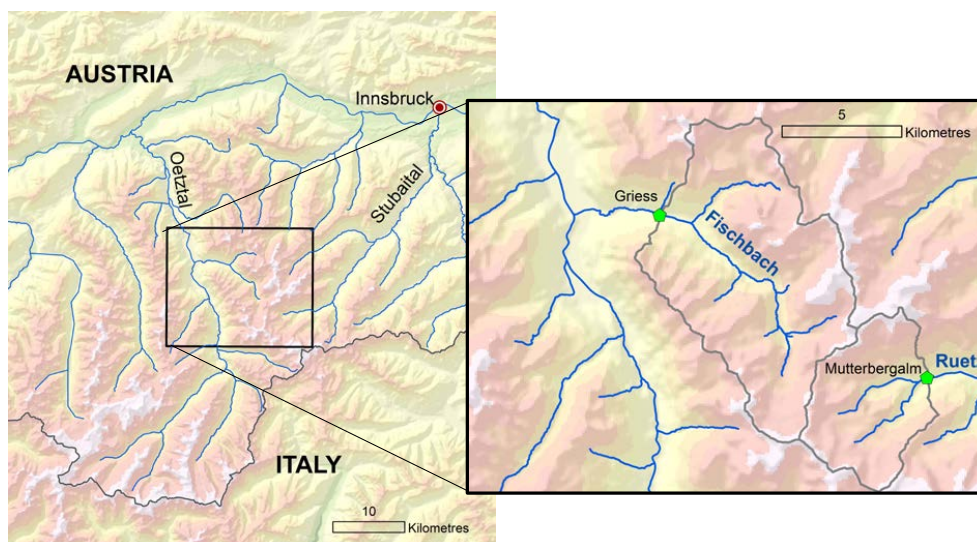


**Figure 1.** Location of the Fischbach and Ruetz mountain stream catchments in the Stubai Alps of Tyrol in western Austria. The measuring sites are indicated with a green pentagon, and the catchment boundaries are marked with a gray line. (Source of topographic map: Abteilung Geoinformation, Amt der Tiroler Landesregierung; <https://www.tirol.gv.at/data>)

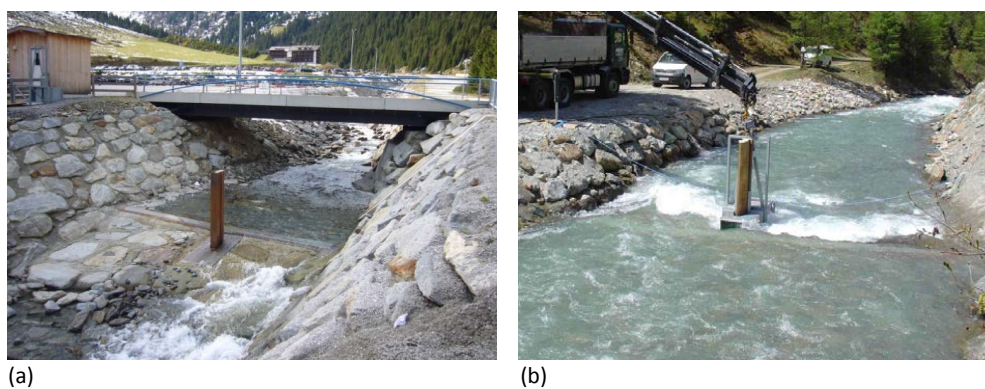


**Figure 2.** Monitoring sites equipped with a Swiss plate geophone system and a flow gauging station. (a) Ruetz, looking upstream onto the sill with the steel plates (28 October 2009), (b) Fischbach, looking downstream during a calibration measurement using the TIWAG basket sampler (27 May 2008). The steel-concrete pillar visible in both photos is used to guide the positioning of the basket sampler during the collection of bedload samples immediately downstream of the geophone plate.

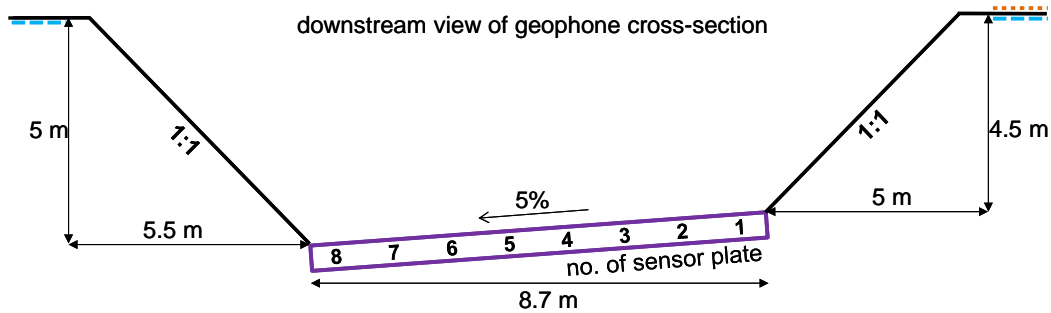


**Figure 3.** Schematic stream cross-section at the geophone measuring site in both Fischbach and Ruetz. The steel-concrete pillar is located downstream of the sensor plate no. 5. The sill with the steel plates is inclined towards the left bank to improve the resolution of the flow gauge measurements at low discharges. On the banks, the dotted horizontal line indicates the paved local road on river right side at the Fischbach, and the two dashed horizontal lines indicate the gravelled parking lot on both river sides at the Ruetz.

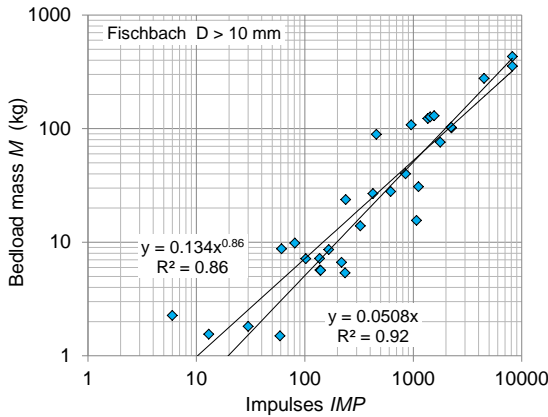


**Figure 4.** Fischbach: Geophone calibration relationships for grains with  $D > 10$  mm between bedload mass  $M$  and number of impulses  $IMP$ . The linear and power law regression equations are based on 31 calibration measurements for the years 2008-2013.

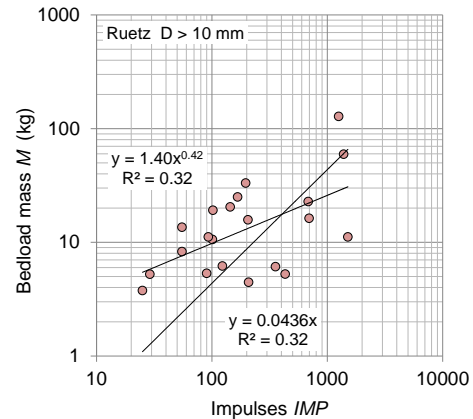


**Figure 5.** Ruetz: Geophone calibration relationships for grains with  $D > 10$  mm between bedload mass  $M$  and number of impulses  $IMP$ . The linear and power law regression equations are based on 21 calibration measurements for the years 2008-2013.

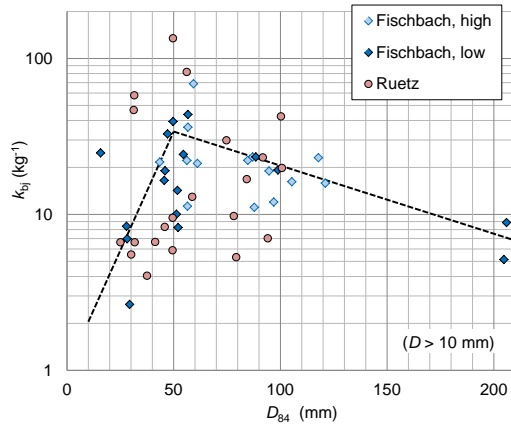


**Figure 6.** Linear calibration coefficient  $k_{bj}$  versus characteristic grain size  $D_{84}$ , determined for particles with  $D > 10$  mm. Fischbach: data points marked “high” and “low” refer to impulse rates higher and lower than  $1 (0.5^{-1} \text{ m}^{-1} \text{ s}^{-1})$ , respectively. The dashed lines are meant to guide the eye.

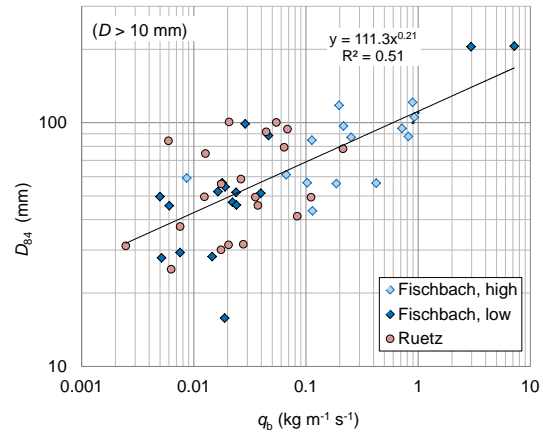


**Figure 7.** Characteristic grain size  $D_{84}$  (determined for particles with  $D > 10$  mm) versus bedload flux  $q_b$ , derived from the calibration bedload samples (for  $D > 10$  mm). Fischbach: data points marked “high” and “low” refer to impulse rates higher and lower than  $1 (0.5^{-1} \text{ m}^{-1} \text{ s}^{-1})$ , respectively. The regression line is based on both the Fischbach and Ruetz data.

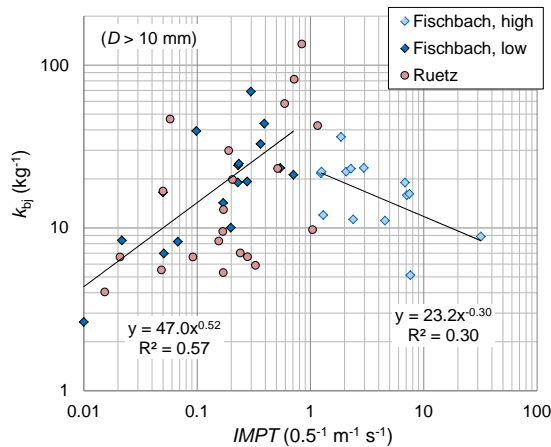


**Figure 8.** Linear calibration coefficient  $k_{bj}$  (for  $D > 10$  mm) versus impulse rate  $IMPT$ . Fischbach: data points marked “high” and “low” refer to impulse rates higher and lower than  $1 (0.5^{-1} \text{ m}^{-1} \text{ s}^{-1})$ , respectively. The regression lines are based on the Fischbach data only.

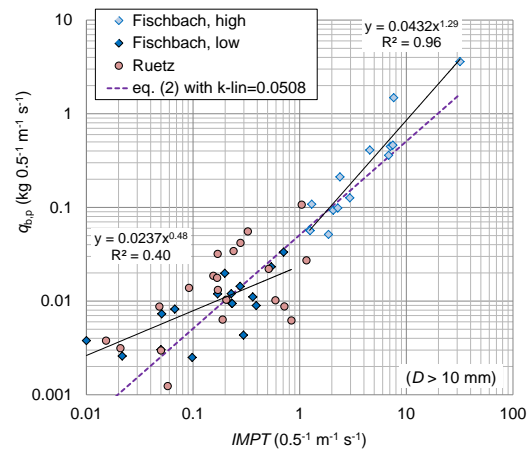


**Figure 9.** Unit bedload transport rate  $q_{b,p}$  for particles  $D > 10$  mm vs. impulse rate  $IMPT$ . Fischbach: data points marked “high” and “low” refer to  $IMPT$  values higher and lower than  $1 (0.5^{-1} \text{ m}^{-1} \text{ s}^{-1})$ , respectively. The regression lines are based on the Fischbach data only. The violet dashed line represents the linear calibration relation Eq. (2) determined for the Fischbach data based on a regression of  $M$  vs.  $IMP$ .

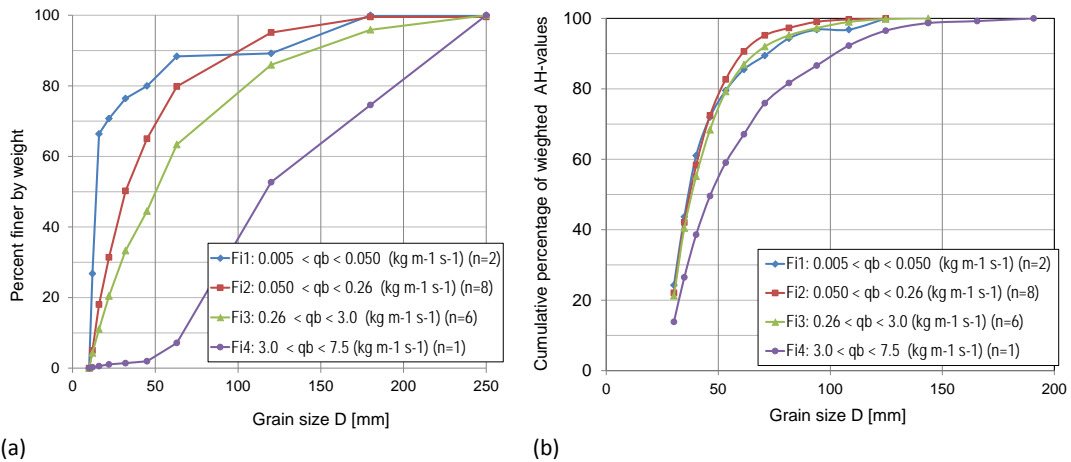


**Figure 10.** Fischbach: (a) Grain size distributions derived from the calibration bedload samples (for  $D > 10$  mm), averaged for four classes of bedload fluxes  $q_b$  (using 17 samples from 2010-2012). (b) Relative distribution of grain sizes estimated from the geophone measurements based on the AH data, averaged for the same four classes of bedload fluxes (using the same 17 sample periods from 2010-2012).

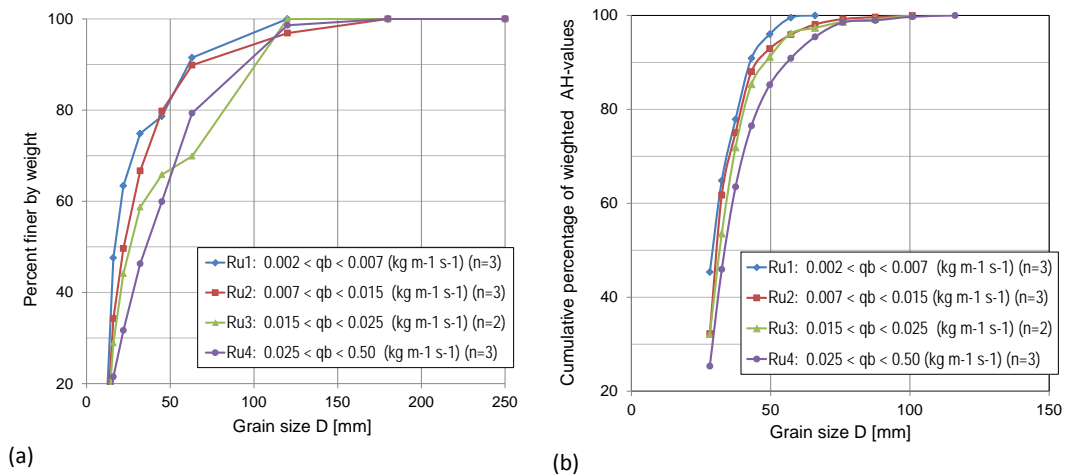


**Figure 11.** Ruetz: (a) Grain size distributions derived from the calibration bedload samples (for  $D > 10$  mm), averaged for four classes of bedload fluxes  $q_b$  (using 11 samples from 2010-2013). (b) Relative distribution of grain sizes estimated from the geophone measurements based on the AH data, averaged for the same four classes of bedload fluxes (using the same 11 sample periods from 2010-2013).



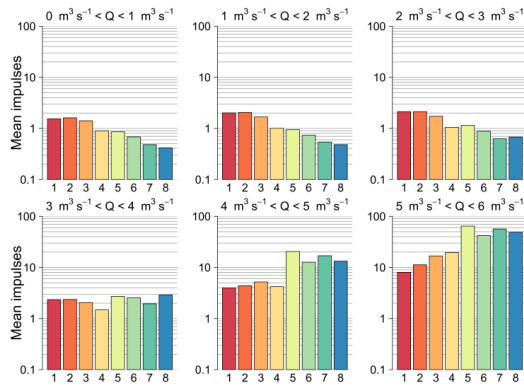


**Figure 12.** Fischbach: Arithmetic mean of geophone impulses per 15 min for each of the eight plates (ordinates), averaged over the period 2008-2013 and including zero values, for discharge  $Q$  classes with width of  $1 \text{ m}^3 \text{ s}^{-1}$ , for discharges up to  $6 \text{ m}^3 \text{ s}^{-1}$ .

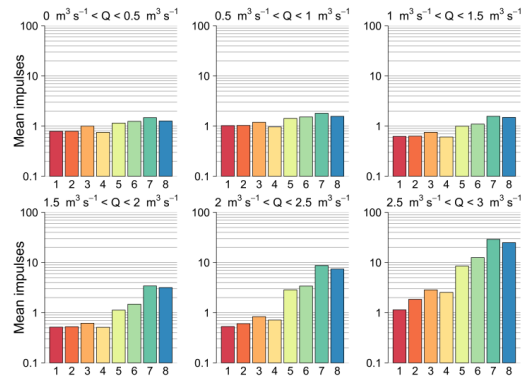


**Figure 13.** Ruetz: Arithmetic mean of geophone impulses per 15 min for each of the eight plates (ordinates), averaged over the period 2008-2013 and including zero values, for discharge  $Q$  classes with width of  $0.5 \text{ m}^3 \text{ s}^{-1}$ , for discharges up to  $3 \text{ m}^3 \text{ s}^{-1}$ .

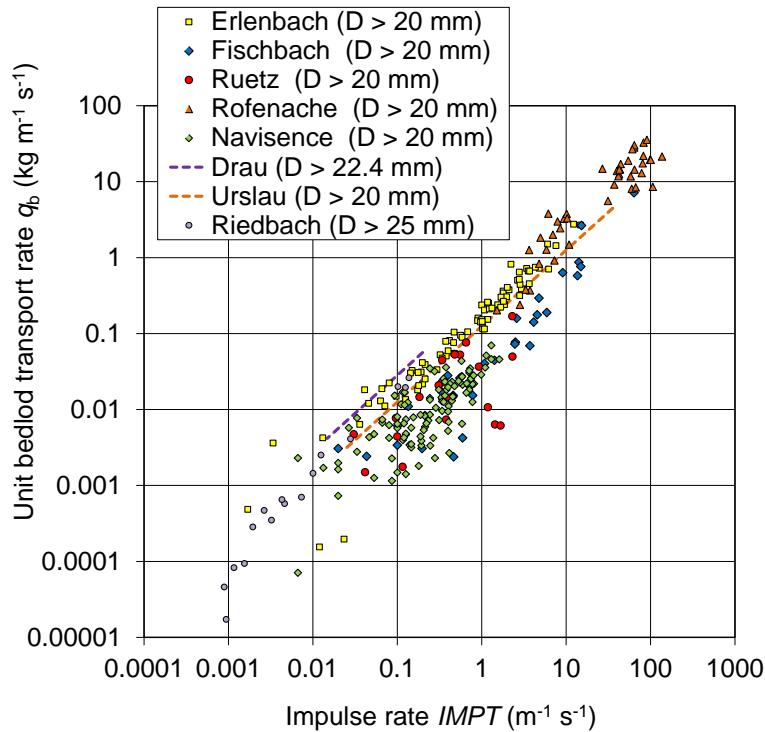


**Figure 14.** Comparison of geophone calibration data from eight different stream sites. Unit bedload transport rate  $q_b$  for particles with  $D$  larger than (mostly) 20 mm is plotted against impulse rate  $IMPT$ . Data sources for additional data are: Wyss et al. (2016c) for Navisence and Erlenbach (some data up to 2016 were added here); Habersack et al. (2016) for Drau; Kreisler et al. (2016) for Urslau (linear calibration relation is approximate;  $q_b$  values given for  $D > 10 \text{ mm}$  were reduced by factor of 0.68 to estimate  $q_b$  values for  $D > 20 \text{ mm}$ ; reduction factor was estimated from 85 samples of Erlenbach moving basket data); Schneider et al. (2016) for Riedbach.

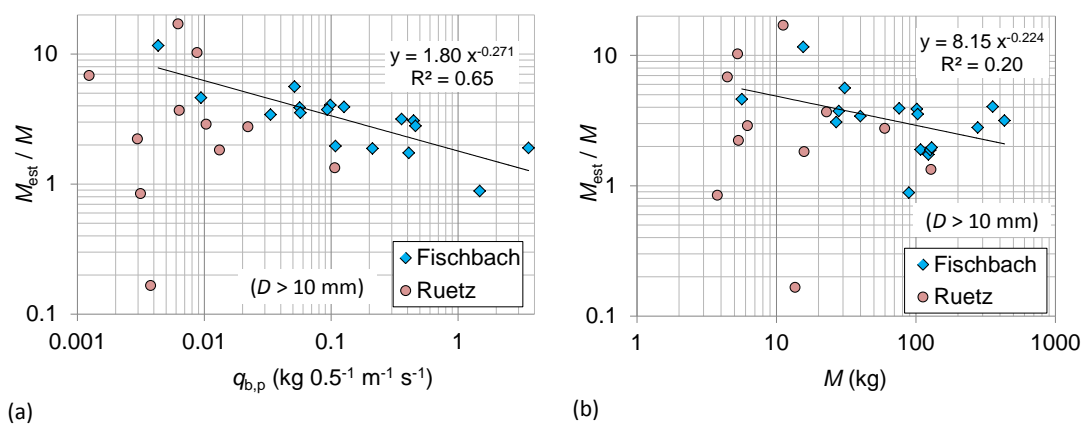


**Figure 15.** The estimated bedload mass per sample using the method in Wyss et al. (2016a) developed for the Erlenbach,  $M_{est}$ , is compared with the measured bedload mass,  $M$ , through the ratio  $M_{est}/M$ . (a) Ratio  $M_{est}/M$  shown vs. unit bedload transport rate  $q_{b,p}$  for particles with  $D > 10$  mm, (b) Ratio  $M_{est}/M$  shown vs. measured bedload Mass  $M$  for particles with  $D > 10$  mm. In both diagrams the regression line is based on the Fischbach data only.